The link between submillimetre galaxies and luminous ellipticals: near-infrared IFU spectroscopy of submillimetre galaxies

A. M. Swinbank,[1]⋆ S. C. Chapman,[2] Ian Smail,[1] C. Lindner,[2] C. Borys,[2,3]
A. W. Blain,[2] R. J. Ivison[4,5] and G. F. Lewis[6]

[1]*Institute for Computational Cosmology, Department of Physics, Durham University, South Road, Durham DH1 3LE*

[2]*Astronomy Department, California Institute of Technology, 105-24, Pasadena, CA 91125, USA*

[3]*University of Toronto, Toronto, Ontario M5S 3H8, Canada*

[4]*Astronomy Technology Center, Royal Observatory, Blackford Hill, Edinburgh EH19 3HJ*

[5]*Institute for Astronomy, University of Edinburgh, Edinburgh EH19 3HJ*

[6]*School of Physics, University of Sydney, NSW 2006, Australia*

ABSTRACT

We present two-dimensional spectroscopy covering the rest-frame wavelengths of strong optical emission lines in six luminous submillimetre galaxies (SMGs) at $z = 1.3$–2.5. Using this near-infrared integral field spectroscopy together with *Hubble Space Telescope* ACS and NICMOS imaging, we map the dynamics and morphologies of these systems on scales from 4–11 kpc. Four of the systems show multiple components in their spatially resolved spectra with average velocity offsets of $\sim$180 km s^{-1} across 8 kpc in projection. From the ensemble properties of eight galaxies, from our survey and the literature, we estimate the typical dynamical masses of bright SMGs as $5 \pm 3 \times 10^{11}$ M$_\odot$. This is similar to recent estimates of their stellar masses – suggesting that the dynamics of the central regions of these galaxies are baryon dominated, with a substantial fraction of those baryons in stars by the epoch of observation. Combining our dynamical mass estimates with stellar luminosities for this population, we investigate whether SMGs can evolve on to the Faber–Jackson (FJ) relation for local ellipticals. Adopting a typical lifetime of $\tau_{\text{burst}} \sim 300$ Myr for the submillimetre-luminous phase – using the latest estimates of gas masses, star formation rates and active galactic nucleus contribution to the bolometric luminosities – we find that the stellar populations of SMGs should fade to place them on the FJ relation, at $M_K \sim -25.1$. Furthermore, using the same starburst lifetime we correct the observed space density of SMGs for the duty cycle to derive a volume density of the progenitors of $\sim$1 × 10^{-4} Mpc^{-3}. This is consistent with the space density of local luminous early-type galaxies with $M_K \sim -25.1$, indicating that SMGs can evolve on to the scaling relations observed for local early-type galaxies, and the observed population at $z \sim 2$ is then sufficient to account for the formation of the whole population of $\gtrsim 3\,L_K^*$ ellipticals seen at $z \sim 0$.

Key words: galaxies: evolution – galaxies: high-redshift – galaxies: individual – submillimetre.

1 INTRODUCTION

Deep optical and near-infrared imaging with the superlative resolution of the NICMOS and ACS cameras on-board *Hubble Space Telescope* (*HST*) has made it possible to study the morphologies and colours of high-redshift far-infrared luminous galaxies identified in the submillimetre (submm) waveband in unprecedented levels of

detail (Smail et al. 1998, 2002; Chapman et al. 2003b; Smail et al. 2004; Almaini et al. 2005; Pope et al. 2005). By combining this data with spectroscopically confirmed redshifts (Chapman et al. 2003a, 2005), we are beginning to understand the processes which triggers the immense bolometric luminosity output in these galaxies, allowing us to address issues such as their true contribution to the star formation rate history of the Universe (e.g. Chapman et al. 2005). Submm galaxies (SMGs) are amongst the most bolometrically luminous galaxies in the Universe (with $L_{\text{bol}} \sim 10^{13}$ L$_\odot$ and a median redshift of $\langle z \rangle \sim 2.2$). However, in contrast to quasars at the same

⋆E-mail: a.m.swinbank@durham.ac.uk

early epochs, their bolometric output appears to be dominated by the star formation rather than AGN activity (Swinbank et al. 2004; Alexander et al. 2005). It is clearly important to establish firmly the masses for these galaxies in order to understanding the rapid evolution of the submm population. Such diagnostics will allow us to determine how they relate to present-day galaxies and in particular to test whether they represent the formation phase of the most massive elliptical galaxies at the present day, as many suspect (Lilly et al. 1999).

To probe the dynamical structures of these frequently complex systems requires a reliable separation of the spatial and spectral information. One particularly powerful approach to achieve this is using millimetric CO emission-line maps to trace the distribution and kinematics of dense gas within the galaxies (Frayer et al. 1999, 2003; Neri et al. 2003; Greve et al. 2005) especially at high resolution (Downes & Solomon 2003; Genzel et al. 2003; Tacconi et al. 2006). Unfortunately, prior to the commissioning of the Atacama Large Millimetre Array, this approach remains observationally very demanding, typically requiring 30 h per source with the IRAM interferometer and can only be applied to the most massive and gas-rich SMGs. An alternative tool which is less demanding in terms of telescope time and can provide spatially resolved dynamics of SMGs with sufficient spatial and velocity resolution to study their internal structure is near-infrared integral field spectroscopy targeting the rest-frame optical emission lines such as [O III]λ5007 and H$\alpha\lambda$6563 (e.g. Tecza et al. 2004; Swinbank et al. 2005). The spectroscopic maps so produced allow us to trace the dynamical and structural properties of SMGs on scales of a few kpc, pin-point the sites of active star formation and identify non-thermal emission from active galactic nuclei (AGN) in components within these systems. However, they are also subject to potential biases due to extreme extinction within some regions of the SMGs and from outflows in the emission-line gas which is being observed (Bower et al. 2004). While the star formation rates estimated from the Hα are typically a factor of 10–100$\times$ less than that predicted from the far-infrared emission (suggesting to 1–4 mag of dust absorption; q.v. Smail et al. 2004), it is clear that the Hα emission provides a more secure probe of the star formation rates and dynamics than either the Lyα emission or rest-frame ultraviolet (UV) continuum and can thus provide a reliable and observationally efficient probe of the activity and dynamics of this important population.

Using the UIST near-infrared integral field unit (IFU) at UKIRT and the GNIRS IFU at Gemini-South we have studied the rest-frame optical emission-line properties of six SMGs at $z = 1.3$–2.5. These observations, together with high-resolution imaging from *HST* allow us to probe the physical cause of the rapid evolution of SMGs,

enabling us to test whether these far-infrared luminous galaxies comprise merging systems which are likely to be the progenitors of local massive ellipticals, or whether instead they are simply high-luminosity episodes in the history of more mundane galaxies. Our paper is laid out as follows. In Section 2, we present the observations and their reduction. In Section 3, we discuss the analysis of these data, while in Sections 4 and 5 we present our discussion and conclusions, respectively. We use a cosmology with $H_0 = 70$ km s^{-1}, $\Omega_M = 0.3$ and $\Omega_\Lambda = 0.7$ in which 1 arcsec corresponds to 8.2 kpc at $z = 2.5$ and 8.5 kpc at $z = 1.5$.

2 OBSERVATIONS AND REDUCTION

The SMGs in this paper come from surveys at 850 or 1200 μm by Scott et al. (2002), Greve et al. (2004) and Webb et al. (2003b). These sources were spectroscopically identified by Chapman et al. (2003a, 2005) and confirmed with precise redshifts from Swinbank et al. (2004) based on accurate radio positions (e.g. Ivison et al. 2002). We also include the recently discovered hyper-luminous far-infrared-selected galaxy MIPS J142824.0+352619 from Borys et al. (2006a) as well as an optically faint radio galaxy (OFRG) which was tentatively detected as a millimeter continuum source in Greve et al. (2005) for which a spectroscopic redshift was measured by Chapman et al. (in preparation). The coordinates and redshifts for each source are reported in Table 1 and we briefly review the properties of each individual source here.

2.1 Sample

CFRS 03.15. First identified in the Canada–UK Deep Submm Survey by Webb et al. (2003a), this SMG has $S_{850} = 4.4 \pm 1.1$ mJy and a 1.4-GHz flux density of $S_{1.4\,GHz} = 226 \pm 12$ μJy. Spectroscopic observations from Chapman et al. (2005) and Swinbank et al. (2004) yield a redshift of $z = 1.4076$ which implies a luminosity of $L_{FIR} = 5.8 \pm 1.5 \times 10^{12} L_\odot$. The rest-frame UV spectroscopy from Chapman et al. (2005) shows strong C IV emission, which along with the high [N II]/Hα line ratio and apparent underlying broad Hα line in the near-infrared spectra from Swinbank et al. (2004) suggests substantial AGN activity.

N2 850.7. This submm-selected galaxy has $S_{850} = 9.0 \pm 2.4$ mJy, lies at $z = 1.488$, and has a far-infrared luminosity of $L_{FIR} = 6.4 \pm 1.7 \times 10^{12} L_\odot$ (Chapman et al. 2005). The existing optical and near-infrared spectroscopy of this source suggest that the bolometric luminosity is predominantly arising from a starburst, with low [N II]/Hα and C IV/Lyα emission line ratios (Swinbank et al. 2004; Chapman et al. 2005). Interferometric observations of the molecular CO emission in this system by Greve et al. (2005) failed to detect

Table 1. Log of IFU observations.

SMG	RA	Dec.	z	t_{exp} (ks)
UIST/UKIRT				
SMM J163639.01+405635.9 (N2 850.7)	16:36:39.40	+40:56:38.0	1.4880	21.6
SMM J163655.80+405914.0 (N2 1200.18)	16:36:55.90	+40:59:12.0	2.5918	21.6
RG J163655.05+410432.0 (N2 1200.90)	16:36:55.05	+41:04:32.0	2.1981	14.4
MIPS J142824.0+352619.0	14:28:24.40	+35:26:21.8	1.328	21.6
SMM J221804.42+002154.4 (SSA 22.96)	22:18:04.43	+00:21:53.2	2.517	10.8
Gemini/GNIRS				
SMM J030227.73+000653.5 (CFRS 03.15)	03:02:27.6	+00:06:52.5	1.4076	7.2

Note. The submm names/position give the 850-μm centroid whilst the RA and Dec. marked denote the 1.4-GHz radio centroid.

the CO(2-1) line. If the gas reservoir within this galaxy is close to the systemic redshift, indicated by the Hα emission line, then this non-detection implies an upper limit of $<1.8 \times 10^{10}$ M$_\odot$ on the H$_2$ gas mass.

N2 1200.18. The near-infrared spectroscopy of N2 1200.18 indicates a redshift of $z = 2.592$ (Swinbank et al. 2004), and its 1200-μm flux density of 2.2 ± 0.6 μJy then corresponds to a far-infrared luminosity of $L_{FIR} = 10.9 \pm 3.0 \times 10^{12}$ L$_\odot$ for a reasonable template spectral energy distribution (SED). The radio flux density ($S_{1.4\,GHz} = 180 \pm 22$ μJy) is relatively strong, suggesting a possible contribution from an AGN. This is confirmed by the existing long-slit optical and near-infrared spectroscopy which shows high [N II]/Hα and C IV/Lyα emission line ratios as well as a broad component underlying the Hα emission line [with full width at half-maximum (FWHM) of 2900 ± 400 km s^{-1}] from a partially obscured AGN (Swinbank et al. 2004; Chapman et al. 2005).

N2 1200.90. The 1.4-GHz map of the ELAIS-N2 field shows a slightly resolved source around this galaxy, with a peak flux density of 47 ± 10 μJy beam^{-1} and a total flux density of 63 ± 21 μJy (Biggs & Ivison 2006). A spectroscopic redshift $z = 2.195$ was measured through the identification of Lyα and C IV emission lines, the ratio of these suggests that weak AGN activity is possible (Chapman et al., in preparation).

MIPS J142824.0+352619. Far-infrared imaging with the *Spitzer* Space Telescope recently uncovered an apparently hyperluminous galaxy at $z \sim 1.325$ (Borys et al. 2006a). Multiwavelength follow-up of this galaxy at submm wavelengths suggests a far-infrared luminosity of $3.2 \pm 0.7 \times 10^{13}$ L$_\odot$. Unlike most other $z > 1$ sources of comparable luminosity, MIPS J142824.0+352619 lacks any trace of AGN activity, and therefore the immense luminosity appears to arise due to a $\gtrsim 5000$ M$_\odot$ yr^{-1} starburst. However, spectroscopic observations in the z band have shown that this galaxy is aligned with a foreground $z = 1.03$ elliptical galaxy, suggesting the possibility of gravitational amplification of the background source. This would provide a much more mundane explanation for the apparently immense luminosity of this galaxy.

SSA 22.96. Rest-frame UV spectroscopy of SSA 22.96 from Chapman et al. (2005) indicates a redshift of $z = 2.517$ from UV absorption features, with little indication of AGN activity. This radio pre-selected galaxy has 850 μm and 1.4-GHz flux densities of $S_{850} = 9.0 \pm 2.3$ mJy and $S_{1.4} = 43.8 \pm 10.1$ μJy which suggests a far-infrared luminosity of $L_{FIR} \sim 8 \times 10^{12}$ L$_\odot$.

Deconvolving the exact contributions from the star formation and AGN activity within these galaxies is difficult using just the UV slit spectroscopy from Chapman et al. (2005). Ideally, we need to use the well-developed spectral indicators based on rest-frame optical emission lines (Veilleux & Osterbrock 1987) which fall in the near-infrared for these high-redshift galaxies (Swinbank et al. 2004). Going one step further, and coupling the spatial coverage from an IFU with coverage around the rest-frame optical emission lines allows us to locate and isolate the components hosting the AGN in these systems, determine dynamical masses, as well as searching for extended haloes and/or companions.

2.2 UIST near-infrared integral field spectroscopy

Spectro-imaging observations of five targets were made with the UIST near-infrared integral field spectrograph on UKIRT. The UIST IFU uses an image slicer to take a 3.3×6.0 arcsec^2 field and divides it into 14 slices of width 0.24 arcsec. The dispersed spectra from the slices are reformatted on the detector to provide 2D spectro-

imaging, in our case using the *HK* grism, at a spectral resolution of $\lambda/\Delta\lambda \sim 1000$ and covering a wavelength range of 1.4–2.4 μm. N2 850.7 and N2 1200.18 we observed between 2004 August 20 and September 04, whilst the remaining targets were observed between 2005 June 25 and 30.[1] All observations were taken at <0.6 arcsec seeing and photometric conditions. Observations were carried out in the standard ABBA configuration in which we chopped by 12 arcsec to blank sky to achieve good sky subtraction. Individual exposures were 240 s and each observing block was 7.2 ks which was typically repeated two or three times; thus the total integration time for each object was 10–20 ks (Table 1).

To reduce the data, we used the relevant ORAC-DR pipeline (Cavanagh et al. 2003) which sky subtracts, extracts, wavelength calibrates, flat-fields, flux calibrates and forms the data cube. To accurately align and mosaic the individual data cubes together, we created white light (wavelength collapsed) images around the redshifted Hα emission line from each observing block and used the peak intensity to centroid the object in the IFU data cube. We then spatially aligned and co-added the individual data cubes to create the final mosaic.

2.3 GNIRS integral field spectroscopy

We used the GNIRS IFU spectrograph to observe the $z = 1.4076$ SMG CFRS 03.15.[2] The GNIRS IFU uses an image slicer to take a 3.2×4.8 arcsec^2 field and divides it into 21 slices of width 0.15 arcsec. By re-arranging the slices end to end at the detector, the IFU allows images to be dispersed into full-length spectra whilst preserving the complete 2D spatial information content. This allows 3D spectroscopy across a contiguous 3.2×4.8 arcsec^2 field at 0.15 arcsec per pixel. We used the *H*-band filter with the 32 lines mm^{-1} grating which results in a spectral resolution of $\lambda/\Delta\lambda \sim 1700$ and records a wavelength coverage of between 1.37 and 1.87 μm. Observations were taken on 2005 October 20 in photometric conditions, but moderate (~ 1.0 arcsec) seeing. We used the same observing strategy as with UKIRT: observations were carried out in the standard ABBA configuration in which we chopped away to sky by 12 arcsec to achieve good sky subtraction. Individual exposures were 600 s and each of the ABBA observing blocks was repeated three times to give a total integration time of 7.2 ks. To flux calibrate the data, we observed the UKIRT standard star FS10. We used the Gemini IRAF package to extract, flat-field and wavelength calibrate the data and used IDL to build and combine the data cubes.

2.4 *HST* optical and near-infrared imaging

HST Advanced Camera for Surveys (ACS) observations of N2 850.7, N2 1200.18 were obtained from the *HST* public
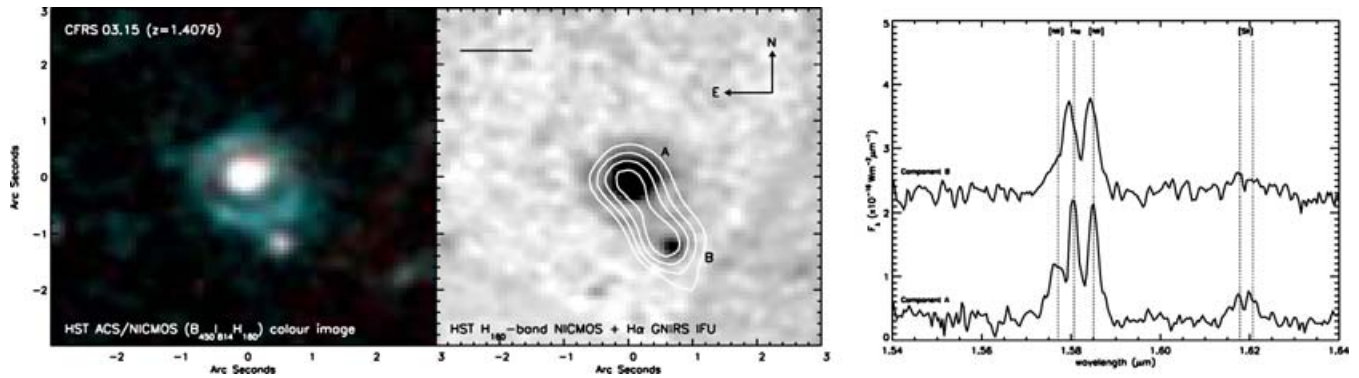
Figure 1. Left-hand panel: true colour *HST* ACS/NICMOS B_{450} I_{814} H_{160}-band image of CFRS 03.15 at $z = 1.4076$ showing the complex morphology (the colour image is displayed in log scale to emphasize the morphology). Middle panel: *HST* NICMOS H_{160}-band image of CFRS 03.15 with the Hα emission-line map from the GNIRS IFU observations overlaid as contours, showing that the bright knot located ∼1.3 arcsec (∼11 kpc) to the south-west is associated with the system. The solid bar represents the FWHM of the seeing disc for the IFU observations. Right-hand panel: spectra from the two components seen in the *HST* imaging of CFRS 03.15 from the Keck/NIRSPEC observation. The top spectrum is offset in flux for clarity. From our spectroscopy, the compact component to the south-west is blueshifted by 90 ± 20 km s^{-1} in projection from the nucleus, suggesting they are two components whose interaction has promoted the strong starburst and disturbed morphology. It is interesting to note that both spectra have strong [N III]/Hα emission-line flux ratios which may indicate that both components host active AGN.

archive[3] (Program ID #9761) whilst ACS images of SSA 22.96 was observed as part of Program #10145. The data consist of dithered exposures with the F814W filter, taken in LOWSKY conditions using the default four-point ACS-WFC-DITHER-BOX configuration. This pattern ensures optimal half-pixel sampling along both coordinates. The typical integration time was 4.8 ks. We reduced the data using the latest version of the MULTIDRIZZLE software (Koekemoer et al. 2002) default parameters with PIXFRAC = 1 and SCALE = 1. The resulting images have 0.05-arcsec pixels and are free from artefacts. Further details of these observations are given in Borys et al. (in preparation) (see also Almaini et al. 2005).

HST WFPC2 observations of CFRS 03.15 were also obtained from the *HST* public archive. The data were taken in the F814W and F450W filters for total of 1.4 ks each (Program ID #05996 and #06556). These observations were reduced using the standard STSDAS package in IRAF.

HST NICMOS observations of N2 850.7 and CFRS 03.15 were obtained in Cycle 12, and the targets were observed using the NIC2 camera in the F160W filter for a total of 2.3 ks (Program ID #9856). We employed the standard four-point spiral dither pattern, LOWSKY conditions and used the MULTIACCUM read-mode. Each exposure was corrected for a pedestal offset, and then mosaiced using the CALNICB task in IRAF. Unfortunately the observation was affected by the South Atlantic Anomaly (SAA), and extra processing steps were required[4]. The final images appear very flat and have very low cosmic ray contamination. The reduction and analysis of these data are described in more detail in Borys et al. (in preparation).

3 ANALYSIS AND RESULTS

3.1 Velocity determinations

To accurately determine the redshift (or velocity offsets between components) in the spectra, we identify and fit both the continuum level and emission lines (e.g. Hαλ6562.8, and [N II]λλ6548.1, 6583.0 where appropriate) simultaneously with a flat continuum plus Gaussian profiles using a χ^2 fit and taking into account the increased noise in regions of strong sky emission. The error bars on the emission-line wavelength in each spectrum are derived by allowing the wavelength of the best-fitting Gaussian profile to vary and allowing the signal to drop by $\Delta \chi^2 = 1$. The quoted error bars are therefore conservative and reflect the signal-to-noise ratio (S/N) of the data. The velocity error is propagated through to the mass determinations in Section 4. However, since the S/N in some of our observations is modest we also attempt to further quantify the error bars on the velocity offsets by creating artificial emission lines at the resolution of the UIST spectrograph. We produce spectra with emission lines with an intrinsic width of 150 km s^{-1} and add Gaussian random noise. We then refit the Gaussian profiles to the data, measuring the velocity offset between the input and output spectrum. Using 10^4 simulations at each S/N, the rms velocity error between the measured fit and the input velocity as a function of S/N is: 140 km s^{-1} at S/N = 3, 100 km s^{-1} at S/N = 5, 65 km s^{-1} at S/N = 7 and 50 km s^{-1} at S/N = 9. As expected, these estimates are comparable to the quoted velocity errors derived using our χ^2 estimate.

Before we discuss what can be learnt from our observations as a whole, we briefly review the results from each of the six galaxies.

3.2 CFRS 03.15

In Fig. 1, we show a true colour *BIH*-band *HST* image of CFRS 03.15. The galaxy shows a compact source surrounded by a diffuse halo of material in a ring-like structure. The colours of the nucleus ($B_{450} - I_{814} = 1.8 I_{814} - H_{160} = 2.5$) are consistent with a star-forming galaxy at $z = 1.407$, although the 'ring' of material surrounding the nucleus is much redder in $(B - I) \gtrsim 3.5$, but bluer in $(I - H) = 1.8 \pm 0.2$, suggesting that [O II]λ3727 emission ($\lambda_{obs} = 8973$ Å) may be contributing significantly to the *I*-band flux. There

[3] Obtained from the Multimission Archive at the Space Telescope Science Institute (MAST). STScI is operated by the Association of Universities for Research in Astronomy, Inc., under NASA contract NAS5-26555. Support for MAST for non-*HST* data is provided by the NASA Office of Space Science via grant NAG5-7584 and by other grants and contracts.
[4] For a full description, see http://www.stsci.edu/hst/nicmos/tools/post_SAA_tools.html.

is also a compact knot (or companion) approximately 1.5 arcsec (12.5 kpc) to the south-west with similar colours to the nucleus.

From our data cube, we construct a wavelength-collapsed Hα image (collapsed between -300 and $+300\,\mathrm{km\,s^{-1}}$ from the systemic redshift of Chapman et al. 2005) and overlay this on the NICMOS *H*-band image (Fig. 1). The *H*-band and Hα morphologies are well matched, and we confirm that the bright knot located ~1.3 arcsec (~11 kpc) to the south-west is associated with the galaxy [the extended Hα morphology and Hα velocity shear were also tentatively detected in the Keck/NIRSPEC spectrum in Swinbank et al. (2004) in which the long slit was placed across both components]. Since the observations were taken in ~1 arcsec seeing, we cannot discuss the small-scale properties of each component in detail (or confirm the nature of the low surface brightness halo of diffuse material surrounding component A), however, these will be discussed in Blain et al. (in preparation) who use laser-guided adaptive optics-assisted *H*-band Keck/OSIRIS IFU observations of this system.

By extracting spectra from around the two brightest components, we identify a velocity offset between the nucleus and the knot of $90 \pm 20\,\mathrm{km\,s^{-1}}$. We note that the [N II]/Hα emission-line flux ratios of components A and B are both high (0.95 ± 0.05 and 1.05 ± 0.05, respectively), suggesting that both components may host active AGN. In order to further search for signatures of non-thermal activity, we attempt to fit each of the spectra with an underlying broad-line component, but the improvement in χ^2 over just fitting [N II]+Hα+[N II] is not significant.

3.3 N2 850.7

We detect Hα emission at 1.630 μm [in agreement with the UV and Hα redshift from Chapman et al. (2005) and Swinbank et al. (2004)] and construct an Hα image of N2 850.7 by collapsing the data cube between 1.620 and 1.640 μm. In Fig. 2, we show the *HST* NICMOS image of N2 850.7 and overlay on this the Hα image from the IFU observations. The Hα morphology of the central com-

ponents is spatially extended and therefore to search for velocity substructure, we extract spectra from the regions in the IFU data cube around the brightest components seen in the *HST* imaging. From each individual component, the S/N of the Hα emission is only modest; nevertheless, it is sufficient to centroid the Hα emission line in all cases and so search for velocity offsets between components. We identify a velocity offset between components A and B of $215 \pm 80\,\mathrm{km\,s^{-1}}$ and an offset between A and C of $135 \pm 90\,\mathrm{km\,s^{-1}}$. The *HST* imaging and velocity offsets suggest that at least two galaxies are undergoing an interaction, although whether component C belongs to the same structure as B (or A) will have to wait for higher resolution (adaptive optics) IFU observations. We note that the continuum colours of A, B and C are very similar (Smail et al. 2004).

Using the Hα luminosity as a star formation rate indicator, we derive star formation rates of 90 ± 20, 70 ± 20 and $60 \pm 20\,\mathrm{M_{\odot}\,yr^{-1}}$ from components A, B and C, respectively (Kennicutt 1998). In comparison, the star formation rate for the whole system from the far-infrared luminosity is $1100 \pm 300\,\mathrm{M_{\odot}\,yr^{-1}}$, implying ~2 mag of extinction (q.v. Smail et al. 2004). We reiterate that neither the emission-line flux ratios from the IFU observations nor the rest-frame UV spectroscopy from Chapman et al. (2005) shows any signs of AGN signatures.

3.4 N2 1200.18

The *HST* I_{814}-band ACS image of N2 1200.18 ($z = 2.5918$) appears complex with a bright knot and a low-surface-brightness extension or companion approximately 0.7 arcsec (6 kpc) to the north. Since the IFU observations of this galaxy cover Hβ, [O III]λ5007 and Hα, we construct wavelength-collapsed images around the [O III]λ5007 and Hα emission lines and overlay these on the NICMOS H_{160}-band image in Fig. 3. The strongest [O III]λ5007 emission appears to come from an unresolved point source in the central, bright I_{814}-band continuum component. In contrast, the Hα is much more extended
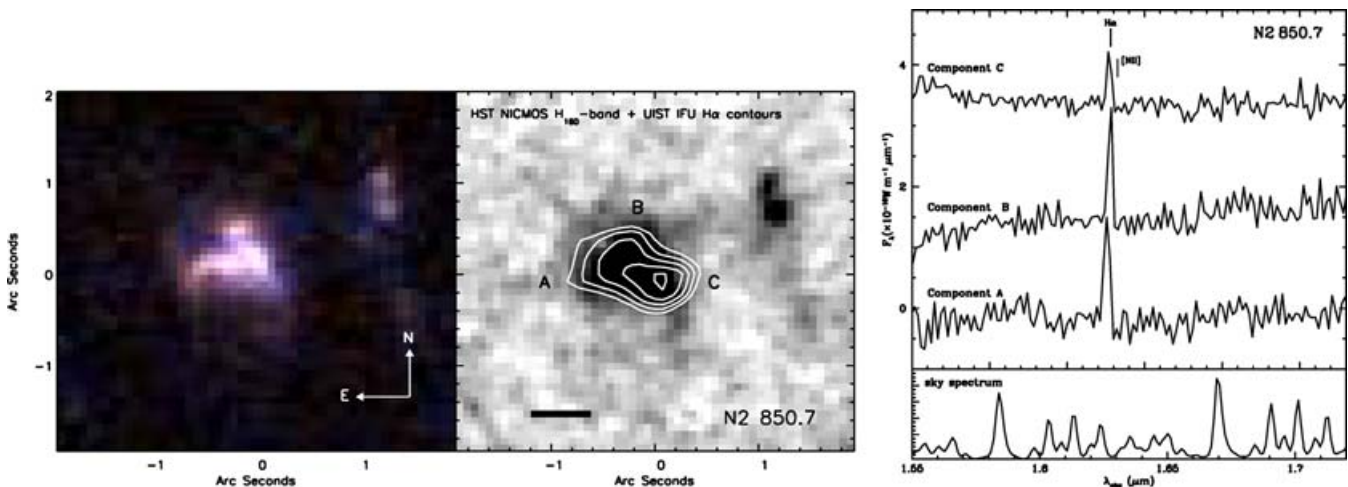

Figure 2. Left-hand panel: a true colour image of N2 850.7 comprising *HST* ACS I_{814}-band and NICMOS H_{160}-band images illustrating the complex morphology of this system. Middle panel: NICMOS H_{160}-band image with Hα emission-line intensity overlaid as contours. Each panel is 4 arcsec^2 (34 kpc at $z = 1.49$) and has east left and north top. The bar shown on the NICMOS image indicates the 0.6-arcsec resolution of the IFU observations. The system comprises at least three components, marked as A, B and C (and there is also tentative evidence for weak Hα emission from the source ~1 arcsec to the west, suggesting it may be associated with the system). The continuum colours of C are bluer than the other components. The intensity of the Hα emission traces the H_{160}-band morphology and it is interesting to note that the star formation appears distributed across the SMG. Right-hand panel: spectra covering the redshifted Hα emission in the three components of N2 850.7 from the UIST IFU observations. The spectra have been offset in flux scale for clarity. The lower panel shows a sky spectrum. By centroiding the emission lines, we find velocity offsets between components A & B and A & C of 215 ± 80 and $135 \pm 90\,\mathrm{km\,s^{-1}}$ in projection, respectively.
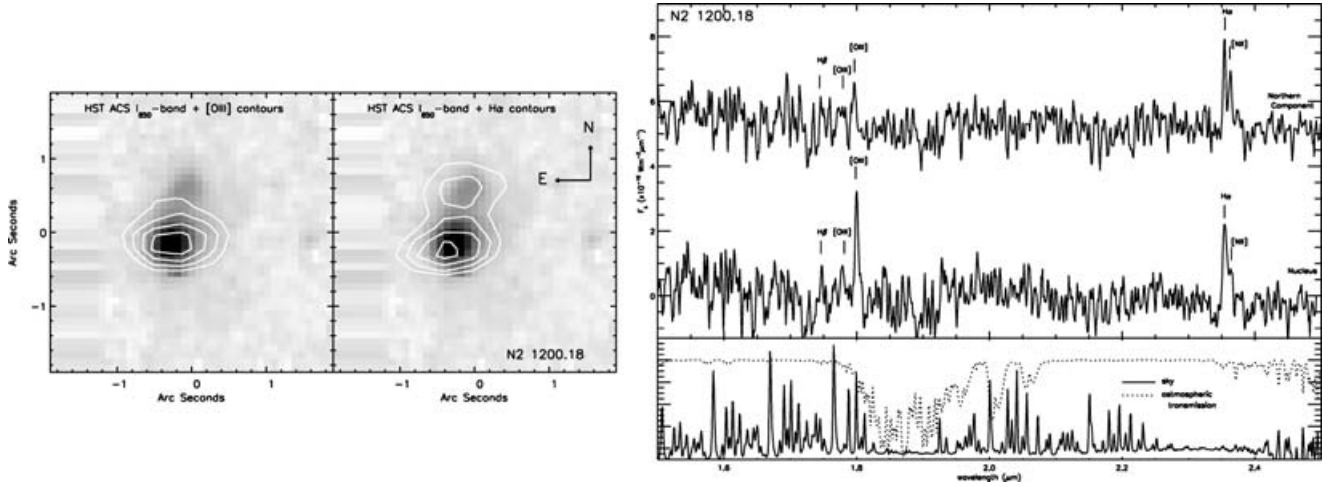
Figure 3. Left-hand panel: *HST* I_{814}-band image of N2 1200.18 with the [O III]λ5007 and Hα emission-line intensity maps from the UIST IFU observations overlaid as contours. Both panels are displayed on a log scale to emphasis the morphology. The *HST* image shows a central bright, compact component and a lower surface brightness extension to the north. The [O III]λ5007 and Hα emission also have different morphologies, with the strong, compact [O III]λ5007 probably arising from (unresolved) AGN activity in the bright central component, whilst the Hα morphology appears resolved and extends across the whole system. Right-hand panel: spectra from the central component and northern extension of N2 1200.18 around the [O III]λ5007 and Hα emission lines from the UIST IFU observations. The spectrum of the central source has an [O III]/Hα emission-line flux ratio of 2.0 ± 0.5 which, combined with the unresolved [O III] emission suggests AGN activity. The northern component has a velocity offset of 250 ± 80 km s^{-1} from the nucleus. This northern component has starburst (rather than AGN) characteristics, with a lower [O III]/Hα and [N II]/Hα emission-line flux ratios. Bottom panel: the OH airglow emission from the sky (continuous line), as well as the Mauna Kea atmospheric transmission (dotted line) are also shown in the lower panel.
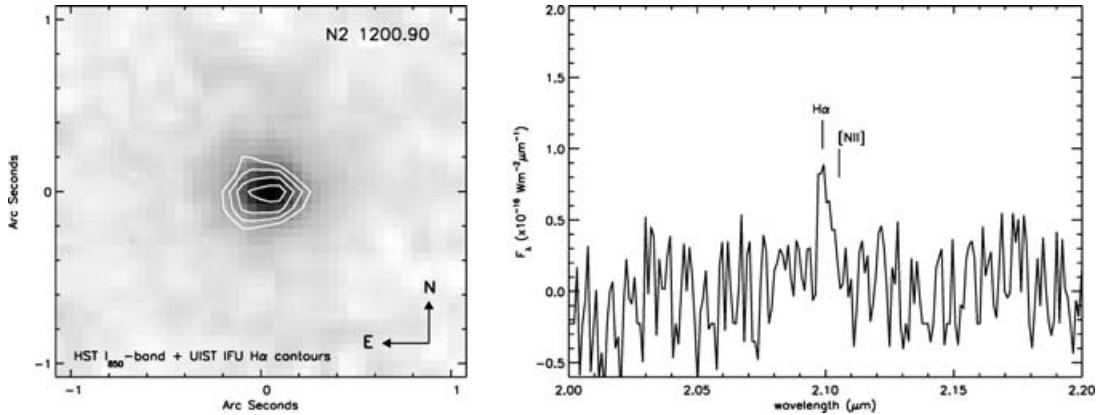

Figure 4. Left-hand panel: *HST* I_{814}-band image of N2 1200.90. The galaxy has a compact morphology [$\lesssim$ 0.2 arcsec (1.6 kpc) FWHM] in this continuum imaging. Right-hand panel: spectrum of N2 1200.90 from the UIST IFU observations showing Hα at a redshift of $z = 2.198$. The rest-frame UV spectrum from Chapman et al. (2006) shows clear signs of AGN activity, yet the apparently low [N II]/Hα emission line ratio from our near-infrared spectroscopy is more suggestive of star formation. However, we note that the Hα emission linewidth of 500 ± 100 km s^{-1} may indicate (non-thermal) AGN activity.

and has features which match the extended Northern component seen in the I_{814}-band. This suggests that the compact continuum source may host an AGN and indeed, both the strong, spatially unresolved [O III]λ5007 and high [O III]λ5007/Hα(=2.0 ± 0.5) and [N II]/Hα(=0.7 ± 0.1) emission line ratios suggest AGN activity. We note that the Hα/Hβ emission-line flux ratio of the central and northern components are 8 ± 3 and >5, respectively.

We can use the emission-line flux ratios of [O III]/Hβ and [N II]/Hα of N2 1200.18 to classify the two components seen in the UIST IFU data. The northern component has an [N II]/Hα emission-line flux ratio of 0.6 ± 0.1, and an [O III]λ5007/Hβ ratio of 0.5 ± 0.2, together these place this component in the low ionisation emission line region (LINER) of the diagnostic diagrams of Baldwin, Phillips & Terlevich (1981). The high [O III]λ5007/Hα and [N II]/Hα emission-line flux ratios from the central unresolved component, indicate a Seyfert-2 type AGN.

Using the velocity derived from the Hα emission, we find that the unresolved central component is redshifted from the northern extended component with a velocity offset of 250 ± 100 km s^{-1} across 0.8 arcsec ($\sim$7 kpc) in projection.

Using deep *Chandra* observations of the ELAIS N2 field, it is also possible to compare the X-ray and spectral properties of N2 1200.18. This galaxy is detected in the hard (2–8 keV) X-ray image with a flux of 14.7 ± 2.1 × 10^{-15} erg s^{-1} cm^{-2} (Manners et al. 2003). We convert the observed 2–8 keV flux to a rest-frame 2–10 keV luminosity using the equations from Alexander et al. (2003b) assuming a spectral index $\Gamma = 2$. We derive $L_X = 9.1 \pm 1.3 \times 10^{44}$ erg s^{-1}. Under the assumption that the [O III]λ5007 emission line and the hard X-ray fluxes are isotropic, they can be used to investigate the intrinsic power of Seyfert galaxies (Mulchaey et al. 1994; Alonso-Herrero, Ward & Kotilainen 1997). N2 1200.18 sits comfortably in the scatter of the $L_{\rm [OIII]}$–L_X plot for local Seyferts

from Mulchaey et al. (1994), although it lies at the high-luminosity end, furthering the suggestion that N2 1200.18 hosts a high-luminosity type 2 Seyfert AGN, and also suggesting that increased AGN activity results in increased photoionization of the surrounding material. This source, along with low-resolution spectroscopy of the [O III]5007 emission from a larger sample of SMGs, is discussed in detail by Takata et al. (in preparation).

3.5 N2 1200.90

The *HST* I_{814} image of this galaxy shows a compact morphology [$\lesssim$0.2 arcsec (1.6 kpc) FWHM], which is matched by the Hα morphology from the UIST IFU observations (Fig. 4). The Hα emission from this galaxy is spatially unresolved and we detect no significant velocity structure across the galaxy. The linewidth of the Hα emission is 420 ± 100 km s^{-1} and the integrated line flux of 0.5×10^{-18} Wm^{-2} then suggests an SFR of 150 ± 50 M$_\odot$ yr^{-1} (Kennicutt 1998).

3.6 MIPS J142824.0+352619

The discovery that there is a fortuitous alignment of a massive foreground elliptical galaxy at $z = 1.03$, superimposed on to the $z = 1.325$ far-infrared-luminous galaxy (Borys et al. 2006a) suggests the possibility that MIPS J142824.0+352619 may be gravitationally lensed. To this end, we targeted the Hα emission with the UIST IFU in order to search for morphological signatures of strong lensing which might explain the apparent immense luminosity of MIPS J142824.0+352619.

In Fig. 5, we show the continuum subtracted Hα emission-line map of MIPS J142824.0+352619 overlaid on the *K*-band continuum image generated from the IFU. The Hα emission is spatially extended, across ~1 arcsec in projection, however, the *H*- and *K*-band light is much more widely distributed, showing likely contamination by light from the foreground lens. The Hα emission appears elongated, but with an alignment which is not naturally ascribed to gravitational lensing (we would expect the brightest images to straddle the long-axis of the foreground lens potential). To search for velocity structure, we extract a series of independent spectra from the data cube along the arc, and place a limit of $\lesssim$125 km s^{-1} on any possible velocity shear. We show the collapsed, one-dimensional spectrum around the Hα emission in Fig. 5. The lack of velocity structure may be a further indication that the Hα morphology arises from two merging images of the same background source,

with the third (much lower surface brightness) image undetectable to the south-west. Whilst such a lens model is somewhat contrived, it would potentially yield an amplification ≫10 for the background source.

3.7 SSA 22.96

The *HST* ACS *I*-band imaging of SSA 22.96 shows several components around the SMG (labelled A). Component A is the radio counterpart in the 1.4-GHz map from Chapman et al. (2004). To align the IFU data cube with the optical imaging, we construct a Hα image of SSA 22.96 by collapsing the data cube between 2.29 and 2.33 μm and overlay this on the *HST* I_{814}-band image in Fig. 6. We extract a spectrum from the data cube around the position of the SMG and also show this in Fig. 6. The Hα redshift of component A is in excellent agreement with the UV redshift from Chapman et al. (2005).

The rest-frame UV spectroscopy from Chapman et al. (2005) is measured from absorption lines, yet the high [N II]/Hα emission-line flux ratio (0.6 ± 0.2) we see may be more consistent with either high metallicity or AGN activity (Veilleux & Osterbrock 1987). We note that this galaxy is not detected in the archival 0.4–10 KeV *XMM* X-ray image of this field to a flux limit of 6×10^{-15} erg s^{-1} cm^{-2} (which corresponds to $L_X < 3 \times 10^{44}$ erg s^{-1}).

4 DISCUSSION

In this paper, we have spatially mapped the rest-frame optical line emission in a sample of six high-redshift, luminous SMGs. We also include in our discussion two similar galaxies which also have published IFU observations (N2 850.4 and SMMJ 14011+0252; Swinbank et al. 2004; Tecza et al. 2004). The most striking feature in the combined sample of eight SMGs is the prevalence of galactic-scale multiple components: five of the eight appear to comprise two or more galactic-scale extensions/components on 1–2 arcsec (8–16 kpc) scales. Our IFU observations also show that the velocity structures can be identified within individual components (e.g. on $\lesssim$ 0.5 arcsec, 4-kpc scales).

Such velocity structures are not only observed through the nebular emission: recently Greve et al. (2005) and Tacconi et al. (2006) have published mm-wavelength observations of 12 SMGs. Several of these systems show double-peaked CO emission-line spectra, with velocity offsets of up to 800 km s^{-1} and linewidths of up to
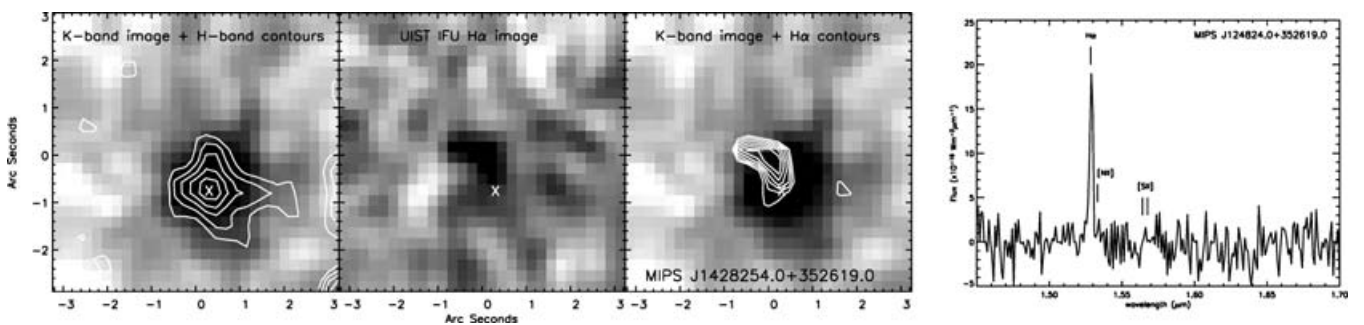

Figure 5. Images of MIPS J142824.0+352619 generated from the UIST IFU observations. Left-hand panel: *K*-band continuum image (collapsed from the data cube between 2.0 and 2.4 μm) with contours overlaid from the *H* band (collapsed between 1.5 and 1.8 μm). Middle panel: continuum-subtracted Hα image. Right-hand panel: *K*-band image with contours from the continuum-subtracted, Hα narrow-band image overlaid. The 'X' in each panel marks the position of the centre of the *H*-band light distribution. In the final panel, we show the collapsed, one-dimensional spectrum around the redshifted Hα emission from MIPS J142824.0+352619. The Hα redshift of $z = 1.328 \pm 0.003$ is in excellent agreement with the CO(5-4) emission, and the Hα linewidth and emission-line flux are also comparable to those given in Borys et al. (2006).
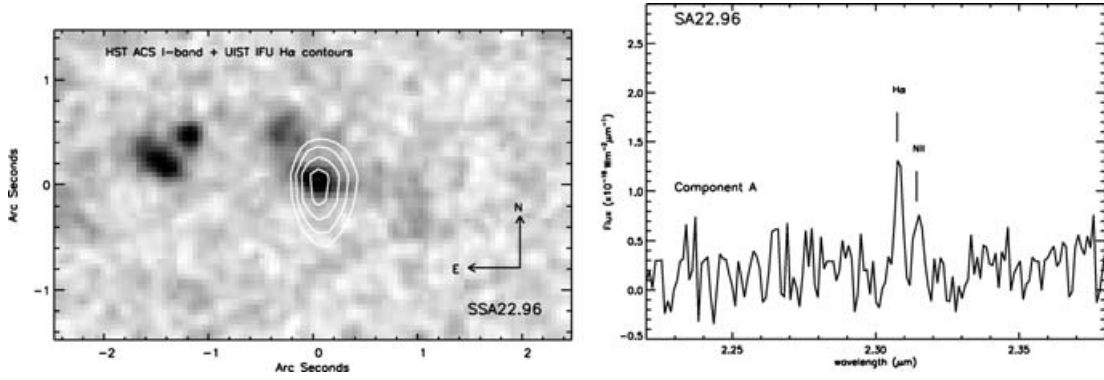
Figure 6. Left-hand panel: *HST* I_{814}-band image of SA 22.96 with the Hα emission from the UIST IFU observations overlaid as contours. Right-hand panel: collapsed spectra around the Hα emission from the western component (A) from the UIST IFU observations of SSA22.96. We identify A as the submm source at redshift $z = 2.517$ through identification of strong Hα and [N II] emission at the same redshift as derived from the rest-frame UV spectroscopy in Chapman et al. (2005). We note that there is tentative evidence for weak Hα emission from the structure ~1.5 arcsec to the east, suggesting it may be associated with the system.

$1000\,\mathrm{km\,s^{-1}}$ (FWHM). The individual CO peaks often have similar intensities ($I_{\mathrm{CO_1}}/I_{\mathrm{CO_2}} = 0.7 \pm 0.1$ with a range of $I_{\mathrm{CO_1}}/I_{\mathrm{CO_2}} = 0.3$–$0.9$) suggesting that many of the SMGs could contain massive gas discs (Genzel et al. 2003). This interpretation is supported by examples of ULIRGS with gas-rich discs in the local Universe (e.g. NGC 6240; Tacconi et al. 1999). However, the obvious interacting/merger nature of many of these distant SMGs from our *HST* and IFU observations strongly suggests that the velocity offsets we measure arise from merging systems. The IFU observations also show that the components have large differences in their energetics and AGN contributions over 2–20 kpc scales.

4.1 Mass estimates

Constraining the stellar, gas and dynamical masses of SMGs is crucial if we have to understand their evolution. Recent dynamical masses for SMGs from CO spectroscopy with millimetre interferometers indicate a dynamical mass of $\log(M_{\mathrm{dyn}}) = 11.1 \pm 0.3$ and gas masses of $\log(M_{\mathrm{gas}}) = 10.5 \pm 0.2$ within the central ~10 kpc (Greve et al. 2005; Tacconi et al. 2006). In addition, estimates of the stellar masses for SMGs have been given by Borys et al. (2006). These are derived by fitting simple stellar population models to the SEDs of SMGs across the rest-frame UV, optical and near-infrared wavebands. The inclusion of rest-frame near-infrared data into these fits improves their insensitivity to dust extinction and thus provides much more reliable measures of the luminosity of the stellar populations in these systems. In this way, Borys et al. (2006) derived a median stellar mass of $\log(M_*) = 11.4 \pm 0.4$ for a small sample of spectroscopically identified SMGs in the GOODS-N region.

We are also able to place limits on their dynamical masses in this population using the projected velocity offsets and spatial separations in our IFU observations. In Fig. 7, we construct a velocity offset versus spatial offset diagram for all SMGs which show multicomponents in their spatially resolved spectra, either from IFU spectroscopy (Tecza et al. 2004; Swinbank et al. 2005; this work); resolved CO spectroscopy (Greve et al. 2005; Tacconi et al. 2006); or long-slit observations (Swinbank et al. 2004). We note that no two data points in Fig. 7 represent the same SMG: the only multicomponent SMG which has both CO and IFU observations (N2 850.4) is represented by an IFU data point in the figure (the measured kinematics in N2 850.4 from IFU and CO observations give consistent
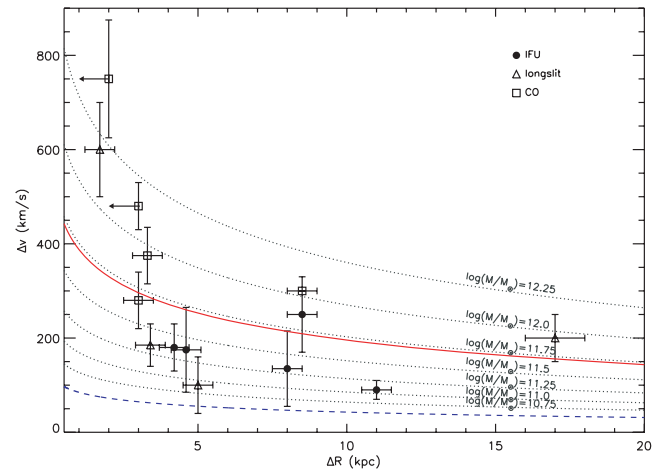

Figure 7. Velocity offset versus spatial offset for the multiple components within SMGs from IFU, long-slit or CO observations. The dotted lines show the expected profiles as a function of halo mass for a galaxy with an NFW profile and a concentration parameter typical of elliptical galaxies. Treating the observations as an ensemble, we derive a dynamical mass for the SMGs of $M = 5 \pm 3 \times 10^{11}\,\mathrm{M_\odot}$ (shown by the solid line). For comparison, the dashed line shows the profile for the minimum stellar mass derived from Borys et al. (2005).

results and are discussed in Swinbank et al. (2005); see also Tacconi et al. (2006)).

To investigate the masses of these systems, we assume that the velocity offsets between the different components eventually transform into motions in a single, relaxed potential well, i.e. they reflect virial motions. We therefore overlay the expected projected velocity dispersion as a function of radius for an elliptical galaxy with an NFW profile (Navarro, Frenk & White 1997; Łokas & Mamon 2001). We assume a concentration of $c = 7$ and a virial radius of 200 kpc – typical of a massive elliptical galaxy (Romanowsky et al. 2003; Mamon & Łokas 2005). Interpreting the velocity offsets in this way, we derive a median dynamical mass of $5 \pm 3 \times 10^{11}\,\mathrm{M_\odot}$ within the virial radius for these galaxies.

Before we compare the dynamical mass estimates with the stellar and gas masses, we note first that there are clearly uncertainties in applying the virial theorem and attempting to measure the mass of

a (non-stationary) merging system. The following caveats must be considered.

(1) Whilst these are merging systems and out of equilibrium, the virial theorem may still be applied if an extra term is included to reflect the moment of inertia of the system (d^2I/dt^2): such that $2T + W = d^2I/dt^2$. Since the moment of inertia is strongly weighted towards large radii ($I \propto \int r^2 dm$), relatively minor parts of the galaxy (such as tidal tails) can have a large impact on I and hence the virial mass estimate. However, in many of these systems, the velocity dispersions (and star formation activity) of the individual components (and the fact that two SMGs appear to comprise double AGN) suggest that we are not measuring velocities for 'minor' components, but rather these are likely to be the dominant components of the merger.

(2) The virial theorem is strictly only valid if the components we observe follow the distribution of mass in the galaxy. Since the components we measure are the likely nuclei of the progenitor galaxies they will be more concentrated (due to dynamical friction) than the overall mass distribution and may produce an underestimate of the dynamical mass.

(3) The virial theorem should only be applied if the merging components have similar mass ratios. The velocity dispersions (and star formation activity) of the individual components we measure are often comparable arguing that the mass ratios of the merging components are similar. It is also useful to note that recent observations of local ($z \lesssim 0.1$) ULIRGs which have shown that galaxies with $L \gtrsim 10^{12}$ L$_\odot$ typically comprise systems of two (or more) interacting components with mass ratios from 1:1 to 1:3 (Dasyra et al. 2006).

To gauge the validity of the mass estimate from the virial theorem, we can make a further estimate of the dynamical masses: if we take the velocity offsets and assume these are point masses (i.e. assume $M = \Delta v^2/\Delta rG$), we derive masses of $2.5 \pm 1.5 \times 10^{11}$ M$_\odot$. We view this estimate as more uncertain than that using the virial estimator since this estimate requires placing all of the mass of the progenitors into point masses on circular orbits. The estimate based on the point-mass model is within the range we quote, and so we consider $5 \pm 3 \times 10^{11}$ M$_\odot$ a reasonable estimate of the mass and its uncertainty in the typical SMG in our sample. However, we note that these estimates would benefit considerably from (high angular resolution) adaptive optics IFU observations coupled with a theoretical study of the distribution of detectable emission-line gas within dusty, merging systems at high redshifts.

4.1.1 Comparison with stellar mass estimates

Borys et al. (2005) estimated rest-frame 2.2-μm luminosities for a sample of spectroscopically confirmed SMGs in the GOODS-N region from broad-band photometry covering *UBVRIzJK*+IRAC 3.6/4.5/5.8/8 μm – which spans the rest-frame UV, optical and near-infrared at the redshifts of their sample, $z = 0.56$–2.91. They found $M_K = -26.8 \pm 0.4$ from their sample of 10 galaxies at $z > 1.5$. They then adopted a typical light-to-mass ratio for the stellar population of $L_K/M = 3.2$, based on an estimated mean age of $\sim$250 Myr from fitting simple stellar population models to the broad-band SEDs, and so derive typical stellar masses of $\log(M_*) = 11.4 \pm 0.4$ (Borys et al. 2006). This is a significant stellar mass for a galaxy at $z \sim 2$ and so Borys et al. (2006) discussed in detail the potential uncertainties in their estimates, in particular whether it is possible to reduce the stellar masses. The most obvious way to achieve this would be to adopt a higher L_K/M ratio, equivalent to assuming a younger age for

the stellar population. However, to achieve an order-of-magnitude reduction, i.e. a light-to-mass ratio of $L_K/M \sim 30$, would require a typical age of $\sim$10 Myrs (Leitherer et al. 1999). Given the observed space density of SMGs, such very young ages and hence high-duty cycles imply very large volume densities for the progenitor population ($\sim 10^{-3}$ Mpc^{-3}) which is at least an order of magnitude greater than the estimates of the masses and clustering of this population (Blain et al. 2004; Chapman et al. 2005).

It is also possible that AGN contribute to the measured 2.2-μm luminosities, leading to an overestimation of the stellar masses. As Borys et al. (2006) point out, the shape of the SEDs for typical SMGs is well described by a stellar model and indeed they remove from their analysis the small number of galaxies for which an AGN is potentially dominant in the rest-frame near-infrared. Nevertheless, we can take an extreme view point and ask if AGN produce all of the luminosity in the reddest bands in these sources, how much would that influence the estimated stellar luminosity? We use the average near-infrared spectral index for QSOs from Simpson & Rawlings (2000), $\alpha = 0.98$, assume that all of the observed 8.0-μm luminosity is arising from the AGN and estimate its contribution to the luminosity at a rest-frame wavelength of $\sim$1.6 μm (where the stellar contribution should peak). Using this set of extreme assumptions, we find a median reduction in the stellar luminosity of only 4×, suggesting that a more realistic estimate taking into account the stellar contribution at 8.0 μm, is likely to yield a change of $\lesssim$2×, within the error range quoted by Borys et al. (2006). It is also worth noting at this point that Alexander et al. (2005) have shown that while AGN are ubiquitous in SMGs, their typical contribution to the bolometric emission is $\lesssim$ 10 per cent suggesting that any contamination to the 2.2-μm flux from AGN activity is minimal and unlikely to bias our result.

Finally, we note that recent stellar population synthesis modelling by Maraston et al. (2006) has shown that thermally pulsating asymptotic giant branch (TP-AGB) stars in post-starburst galaxies can contribute significantly to the rest-frame *K*-band luminosity on $\gtrsim$ 200–1000 Myr time-scales. Indeed, the predicted stellar light-to-mass ratios at 250 Myr is $L_K/M \sim 6$–8 (Maraston 1998; Maraston et al. 2006) and therefore may act to reduce our estimated stellar mass by a factor of up to 3× if the luminosity-weighted stellar populations in the SMGs are dominated by stars with ages of $\gtrsim$ 200–1000 Myr. However, in the case of an on-going starburst (as is relevant for SMGs) the importance of TP-AGB phase is likely to be lessened and we estimate a maximum of $L_K/M \sim 5$ at 450 Myr and more typically $L_K/M \lesssim 4$ for the likely ages of SMGs, suggesting that this phase is unlikely to bias our results significantly.

Hence, unless there is a conspiracy between a number of factors, it appears unlikely that the estimated stellar masses for the submillimetre population are overestimated by more than a factor of 2–3×. We conclude therefore that the typical stellar and dynamical masses for SMGs are likely to be similar in magnitude. We estimate a mass ratio of $M_{dyn}/M_* \sim 2$, with a considerable uncertainty. This suggests that, as with local luminous ellipticals, the central regions of these galaxies are baryon dominated.

4.2 Space densities and comparison with local populations

In order to test the connection between SMGs and local galaxy populations, we can evolve their stellar populations to the present day and determine whether their descendents would be consistent with scaling relations for local galaxies, such as the Faber–Jackson (FJ) relation (Faber & Jackson 1976). This will test claims that SMGs evolve into massive ellipticals at the present day (e.g. Lilly et al.

1999). The velocity offsets we measure in Section 4.1 implies an average velocity dispersion of approximately $\sigma = 240 \pm 80$ km s^{-1}. The FJ relation for local early-type galaxies indicates that this dispersion corresponds to an r-band magnitude of $M_r = -22.7 \pm 0.5$ (Bernardi et al. 2005) or $M_K = -25.3 \pm 0.5$ [assuming $(r - K) = 2.6$, typical for an elliptical galaxy at the present day]. Is the expected fading of the stellar populations within the SMGs, with $M_K = -26.8 \pm 0.4$ at $z \sim 2$, sufficient to reconcile them with the $z = 0$ FJ relation?

The key to estimating the degree of fading of the SMGs is to determine the likely ages of the stellar populations. Since the starburst lifetimes in SMGs depend on the mass of the molecular gas reservoir and the star formation rate, Greve et al. (2005) used CO(3-2) transitions for 18 SMGs (and assuming a CO–H$_2$ conversion factor) to infer gas masses, obtaining $M(H_2) \sim 3 \times 10^{10}$ M$_\odot$. Recently, Hainline et al. (in preparation) have reported CO(1-0) observations of an SMG using the Green Bank Telescope and derive an H$_2$ gas mass four times larger than that from the CO(4-3) transition of the same source (implying that $J_{upper} > 3$ transitions of CO significantly underestimate the mass of cold, diffuse molecular gas in SMGs). This suggests that the typical gas masses of SMGs are likely to be $M(H_2) \sim 1 \times 10^{11}$ M$_\odot$. Star formation rates can be derived from the bolometric emission of the source, assuming this is powered by star formation. Greve et al. (2005) used 850 µm and 1.4-GHz fluxes and assumed the far-infrared–radio correlation to determine bolometric luminosities for their sample. They then assumed a conservative contribution of 50 per cent to the bolometric luminosity from an AGN, and so estimated a median star formation rates of 700 M$_\odot$ yr^{-1} for the galaxies in their sample (integrating the Salpeter IMF between 1 and 120 M$_\odot$ yr^{-1}). Two recent results influence this conclusion, but essentially leave it unchanged. First, Alexander et al. (2005) have shown that while AGN are ubiquitous in SMGs, their typical contribution to the bolometric emission is $\lesssim 10$ per cent, which would increase the star formation rate estimated by Greve et al. (2005) by $\sim 2\times$. However, Kovacs et al. (2006) have used 350-µm photometry to improve the estimates of the bolometric luminosities from the far-infrared SEDs of SMGs and show that the star formation rates may be overestimated by a factor of $\lesssim 2\times$, cancelling this increase. Hence, our current best estimate of the gas consumption time-scales in SMGs is: $\tau_{SMG} \sim M(H_2)/SFR \sim 1 \times 10^{11}$ M$_\odot$/700 M$_\odot$ yr^{-1} ~ 150 Myr, although this estimate clearly has significant uncertainties. The reader should note that a burst with this duration and star formation rate can account for all of the observed stellar mass in a typical SMG, suggesting that the activity we are witnessing is likely to be the origin of the majority of the stellar mass in these galaxies (Smail et al. 2004).

We can next compare these burst lifetimes with those required in order for the SMGs to lie on the FJ relation at the present day using stellar synthesis modelling. For SMGs with $z > 1.5$, the average rest-frame K-band magnitude from Borys et al. (2006) is $M_K = -26.8 \pm 0.4$. We start by calculating the fading of a simple instantaneous burst to the present day. We use STARBURST99 (Leitherer et al. 1999) with a Salpeter IMF (Salpeter 1955) and an instantaneous starburst which predicts that between 100 Myr and 10 Gyr there should be approximately $\Delta M_K = 3.4$ mags of fading suggesting the present-day descendants should have $M_K \sim -23.4 \pm 0.4$. This is approximately 2-mag fainter than the FJ relation, given the expected velocity dispersion as found in Section 4.1. Similarly, an instantaneous burst using the models of Maraston et al. (2006) suggests that the fading between 100 Myr and 10 Gyr is approximately $\Delta M_K = 2.1$–2.4 (depending upon the metallicity) – which

is still $\gtrsim 0.6$ mag fainter than the FJ prediction, given our expected velocity dispersion.

However, these instantaneous burst models are unphysical for SMGs which are still forming stars at the current epoch. So, we derive the fading from a more realistic model: a constant burst of star formation of duration 100, 200 and 300 Myr using PEGASE (Le Borgne et al. 2004). For a 100-Myr burst (observed at 50 Myr, since we expect on average to see SMGs half way through their active phase), the fading between the epoch of observation and the present day is $\Delta M_K = 3.2$, ~ 1.5 mag too faint compared to the FJ relation for the velocity dispersion. Taking longer burst durations of 200 and 300 Myr (observed at 100 and 150 Myr respectively) the fading is $\Delta M_K = 2.7$ and 2.3 mag respectively – approximately 1.2 and 0.8 mag off the FJ relation. Thus for our preferred burst lifetime, 300 Myr, observed half way through the burst, the predicted present-day magnitude is $M_K \sim -24.5 \pm 0.4$ compared to the $z = 0$ value of $M_K = -25.3 \pm 0.5$ from the FJ relation.

These predictions are of course sensitive to the choice of IMF, changing from a Salpeter to a Kroupa IMF and for a 300-Myr burst the predicted fading reduces to $\Delta M_K = 1.7$, indicating a present-day luminosity of $M_K \sim -25.1 \pm 0.4$ and placing the SMGs within ~ 0.2 mag of the $z = 0$ FJ relation. We note that such a change would be at odds with the 'top-heavy' IMF needed in semi-analytic models of galaxy formation to reproduce the basic properties of SMGs (e.g. Baugh et al. 2005; see also Blain et al. 1999a,b).

Hence, whilst there are a number of uncertainties in estimating both the starburst lifetimes and the fading of SMGs to the present day, longer burst durations (~ 300 Myr) are favoured in order for SMGs to evolve towards the scaling relations for elliptical galaxies at the present day. Burst time-scales of this length are also consistent with the expected time to consume the gas reservoirs in these galaxies and with the build-up of the present stellar mass in the systems.

We can also investigate how the SMG burst lifetimes influence the space densities of their expected descendants at the present day. The full SMG redshift distribution from Chapman et al. (2005) is well fit by a Gaussian with a mean redshift of $\langle z \rangle = 2.2$ and with, $\sigma_z \sim 1.3$ (accounting for incompleteness in the spectroscopic desert). Thus, the SMGs populate an epoch of about $\tau_{obs} = 1.5$ Gyr in duration. Since $\phi = \rho_{SMG} \tau_{obs}/\tau_{burst}$ (where ϕ is the comoving space density of the descendant population, τ_{burst} is the burst lifetime and ρ_{SMG} is the observed space density) an estimate of τ_{burst} allows us to infer ϕ. We first estimate the observed space density (ρ_{SMG}) by taking the observed surface density of >5 mJy SMGs from Chapman et al. (2005) (~ 1000 per square degree) which suggests that between $z = 0.9$–3.5 the volume density should be $\sim 2.5 \times 10^{-5}$ Mpc^{-3} (this calculation assumes that 67 per cent of the SMGs lie within the 1σ limits and includes the incompleteness correction in both the redshifts and radio-detection limits). Using our estimated lifetime of $\tau_{burst} \sim 300$ Myr, the corrected space density (assuming a galaxy only goes through one SMG phase in its lifetime) is therefore $2.5 \times 10^{-5} \times 1.5$ Gyr/300 Myr $\sim 1.3 \times 10^{-4}$ Mpc^{-3} for a population with predicted present-day K-band absolute magnitude of $M_K \sim -25.1$. Integrating down the $z = 0$ luminosity function of early-type galaxies from Croton et al. (2005) (see also Wake et al., in preparation), to a median magnitude of $M_K \sim -25.1$ we determine a space density of 9×10^{-5} Mpc^{-3} (we note that using the luminous red galaxy luminosity function from Wake et al. 2006 we obtain 1.1×10^{-4} Mpc^{-3}). Thus if SMGs have burst durations of approximately 300 Myr, as indicated by their gas consumption time-scales, then their predicted

fading would place them on (or near-to) the present-day FJ relation and the observed space density of this population at $z \sim 2$ (corrected for the duty-cycle of the bursts) would account for the formation of the whole population of early type galaxies with $M_K < -25.1$, ($\gtrsim 3 \, L_K^*$) seen at $z \sim 0$.

Further evidence for the evolution of SMGs into massive ellipticals has also be presented in Tacconi et al. (2006) who used high-resolution millimeter imaging to derive matter volume and surface densities of $\sim 100 \, cm^{-3}$ and $5000 \, M_\odot \, pc^{-2}$ for the SMGs, comparable to those in massive local ellipticals and Sa bulges. Similarly, Blain et al. (2004) provided tentative evidence for clustering of SMGs at a level consistent with the progenitors of $> L^*$ elliptical galaxies. These provide additional support for our conclusion that SMGs can be connected through a self-consistent evolutionary model to the local luminous galaxy population, which reproduces both the mass–luminosity relationship and luminosity distributions of local elliptical galaxies.

5 CONCLUSIONS

In this paper, we have studied the rest-frame optical emission-line structures and dynamics of six high-redshift, luminous SMGs. Including two sources from the literature with similar observations, we find that of the eight SMGs with resolved spectroscopy, at least five appear to comprise two or more dynamical subcomponents. The average velocity offsets between these components is $\sim 180 \, km \, s^{-1}$ across a projected spatial scale of 8 kpc. The obvious merging/interacting nature of these systems suggests there are analogous to the multicomponent nature of the, typically less bolometrically luminous and slightly more compact, ULIRGs in the local Universe.

Since our IFU observations allow us to disentangle AGN and starburst-like components (e.g. from [N II]/Hα flux ratios), it is perhaps significant that two of the eight SMGs show possible signs of AGN activity in two spatially resolved components on 1-2 arcsec (10–20 kpc) scales. Deep X-ray surveys of the *Chandra* Deep Field North have produced similar results: Alexander et al. (2003a) report that two of seven SMGs in this region are individually associated with pairs of X-ray sources on similar spatial scales (approximately one galactic diameter). Since the chance of a false association is $\lesssim 1$ per cent, it may be that we are witnessing the interaction or merging of AGNs in these sources (a low-redshift example of this binary AGN activity is seen in the ULIRG NGC 6240; Komossa et al. 2003). The double AGN in some of these systems, suggests mergers may be responsible for disturbing the gas orbits in both components, hence fuelling subsequent AGN growth which currently lags behind a significant pre-existing stellar population (Alexander et al. 2003a; Smail et al. 2003).

By combining the spatially resolved kinematic information from IFU, CO and long-slit observations and assuming the velocity offsets we measure are eventually transformed into velocity dispersions in a pressure-supported galaxy, we derive dynamical masses of $5 \pm 3 \times 10^{11} \, M_\odot$ for typical luminous SMGs. This is similar to the dynamical masses found using Hα linewidths (Swinbank et al. 2004) and resolved CO spectroscopy (Greve et al. 2005; Tacconi et al. 2006) and a factor of $\sim 2 \times$ greater than the recent stellar mass estimates from Borys et al. (2006), suggesting that the central regions of these galaxies are baryon dominated.

We combine our dynamical measurement with estimates of the stellar luminosities for this population from Borys et al. (2006). We use these to constrain their likely evolution and so compare the properties expected for the descendents of SMGs with $z = 0$ galaxy

populations. We update the gas depletion time-scales estimated by Greve et al. (2005) using recent results on the gas masses, bolometric luminosities and AGN contributions for this population, deriving typical gas depletion times of ~ 150 Myr. Adopting a typical burst duration of twice this age, ~ 300 Myr, we predict the evolution of their stellar populations and compare these to the FJ relation for local ellipticals. For a ~ 300 Myr burst with a Kroupa IMF, we find that the expected fading would result in the descendents of the SMGs lying within ~ 0.2 mag of the FJ relation at their measured velocity dispersion. The same estimate of the lifetime can be used to correct the apparent space density of SMGs (assuming a galaxy only goes through one SMG phase in its lifetime) to derive a space density for the descendents of this population of $\sim 1.3 \times 10^{-4}$ Mpc^{-3} for a population with $z = 0$ absolute luminosities of $M_K \sim -25.1$. Hence if SMGs have burst durations of ~ 300 Myr, as indicated by gas consumption time-scales, then their predicted fading places them close to the present-day FJ relation. Moreover, the observed population at $z \sim 2$ is very comparable to that of luminous ellipticals with $M_K \lesssim -25.1$ ($\sim 3 \, L_K^*$) at the present day.

Our observations show the power of using integral field spectroscopy around the rest-frame optical emission lines to probe the dynamics and power sources of these galaxies on $\gtrsim 5$ kpc scales. With forthcoming adaptive optics integral field spectroscopy on 8- and 10-m telescopes (e.g. OSIRIS on Keck, NIFS on Gemini and SINFONI on the VLT), we will soon be able to probe the dynamics, metallicities and star formation properties on $\lesssim 0.1$ arcsec (subkpc at $z = 2$) scales. Furthermore, the increased light grasp of large aperture telescopes will allow us to spatially resolve and map the absorption line spectra of these galaxies (including important diagnostic lines such as Ca II H& K, CH *G*-band, Hδ and MgB), allowing us to accurately probe the stellar contents and metallicity gradients, and so investigate the stellar ages and populations produced in these extreme systems. Such observations will allow us to probe further the time-scales involved in the encounters as well as how and when these galaxies form most of their stars and thus the precise relation to similarly massive galaxies at the present-day luminous ellipticals.

REFERENCES

Alexander D. M. et al., 2003a, AJ, 125, 383
Alexander et al., 2003b, AJ, 126, 539
Alexander D. M., Smail I., Bauer F. E., Chapman S. C., Blain A. W., Brandt W. N., Ivison R. J., 2005, Nat, 434, 738
Almaini O., Dunlop J. S., Conselice C. J., Targett T. A., Mclure R. J., 2005, MNRAS, submitted (astro-ph/0511009)
Alonso-Herrero A., Ward M. J., Kotilainen J. K., 1997, MNRAS, 288, 977

Baldwin J. A., Phillips M. M., Terlevich R., 1981, PASP, 93, 5

Baugh C. M., Lacey C. G., Frenk C. S., Granato G. L., Silva L., Bressan A., Benson A. J., Cole S., 2005, MNRAS, 356, 1191

Bernardi M., Sheth R. K., Nichol R. C., Schneider D. P., Brinkmann J., 2005, AJ, 129, 61

Biggs A., Ivison R. J. 2006, MNRAS, submitted

Blain A. W., Jameson A., Smail I., Longair M. S., Kneib J.-P., Ivison R. J., 1999a, MNRAS, 309, 715

Blain A. W., Smail I., Ivison R. J., Kneib J.-P., 1999b, MNRAS, 302, 632

Blain A. W., Chapman S. C., Smail I., Ivison R., 2004, ApJ, 611, 725

Borys C., Smail I., Chapman S. C., Blain A. W., Alexander D. M., Ivison R. J., 2005, ApJ, 635, 853

Borys C. et al., 2006, ApJ, 636, 134

Bower R. G. et al., 2004, MNRAS, 351, 63

Cavanagh B., Hirst P., Jenness T., Economou F., Currie M. J., Todd S., Ryder S. D., 2003, in Payne H. E., Jedrzejewski R. I., Hook R. N., eds, ASP Conf. Ser. Vol. 295, Astronomical Data Analysis Software and Systems XII. Astron. Soc. Pac., San Francisco, p. 237

Chapman S. C., Blain A. W., Ivison R. J., Smail I. R., 2003a, Nat, 422, 695

Chapman S. C., Windhorst R., Odewahn S., Yan H., Conselice C., 2003b, ApJ, 599, 92

Chapman S. C., Smail I., Windhorst R., Muxlow T., Ivison R. J., 2004, ApJ, 611, 732

Chapman S. C., Blain A. W., Smail I., Ivison R. J., 2005, ApJ, 622, 772

Croton D. J. et al., 2005, MNRAS, 356, 1155

Dasyra K. M. et al., 2006, ApJ, 638, 745

Downes D., Solomon P. M., 2003, ApJ, 582, 37

Faber S. M., Jackson R. E., 1976, ApJ, 204, 668

Frayer D. T. et al., 1999, ApJ, 514, L13

Frayer D. T., Armus L., Scoville N. Z., Blain A. W., Reddy N. A., Ivison R. J., Smail I., 2003, AJ, 126, 73

Genzel R., Baker A. J., Tacconi L. J., Lutz D., Cox P., Guilloteau S., Omont A., 2003, ApJ, 584, 633

Greve T. R., Ivison R. J., Bertoldi F., Stevens J. A., Dunlop J. S., Lutz D., Carilli C. L., 2004, MNRAS, 354, 779

Greve T. R. et al., 2005, MNRAS, 359, 1165

Ivison R. J. et al., 2002, MNRAS, 337, 1

Kennicutt R. C., 1998, ARA&A, 36, 189

Koekemoer A. M., Fruchter A. S., Hook R. N., Hack W., 2002, in Arribas S., Koekemoer A., Whitmore B., eds, The 2002 *HST* Workshop. STSI, Baltimore, MD, p. 339

Komossa S., Burwitz V., Hasinger G., Predehl P., Kaastra J. S., Ikebe Y., 2003, ApJ, 582, L15

Kovacs A., Chapman S. C., Dowell C., Blain A., Smail, Ivison R. J., Phillips T. G., 2006, ApJ, in press

Le Borgne D., Rocca-Volmerange B., Prugniel P., Lançon A., Fioc M., Soubiran C., 2004, A&AP, 425, 881

Leitherer C. et al., 1999, ApJS, 123, 3

Lilly S. J., Eales S. A., Gear W. K. P., Hammer F., Le Fèvre O., Crampton D., Bond J. R., Dunne L., 1999, ApJ, 518, 641

Łokas E. L., Mamon G. A., 2001, MNRAS, 321, 155

Mamon G. A., Łokas E. L., 2005, MNRAS, 363, 705

Manners J. C. et al., 2003, MNRAS, 343, 293

Maraston C., 1998, MNRAS, 300, 872

Maraston C., Daddi E., Renzini A., Cimatti A., Dickinson C., Papovich C., Pasquali N., Pirzkal N., 2006, ApJ, submitted (astro-ph/0604530)

Mulchaey J. S., Koratkar A., Ward M. J., Wilson A. S., Whittle M., Antonucci R. R. J., Kinney A. L., Hurt T., 1994, ApJ, 436, 586

Navarro J. F., Frenk C. S., White S. D. M., 1997, ApJ, 490, 493

Neri R. et al., 2003, ApJ, 597, L113

Pope A., Borys C., Scott D., Conselice C., Dickinson M., Mobasher B., 2005, MNRAS, 358, 149

Romanowsky A. J., Douglas N. G., Arnaboldi M., Kuijken K., Merrifield M. R., Napolitano N. R., Capaccioli M., Freeman K. C., 2003, Sci, 301, 1696

Salpeter E. E., 1955, ApJ, 121, 161

Scott S. E. et al., 2002, MNRAS, 331, 817

Simpson C., Rawlings S., 2000, MNRAS, 317, 1023

Smail I., Ivison R. J., Blain A. W., Kneib J.-P., 1998, ApJ, 507, L21

Smail I., Ivison R. J., Blain A. W., Kneib J.-P., 2002, MNRAS, 331, 495

Smail I., Chapman S. C., Ivison R. J., Blain A. W., Takata T., Heckman T. M., Dunlop J. S., Sekiguchi K., 2003, MNRAS, 342, 1185

Smail I., Chapman S. C., Blain A. W., Ivison R. J., 2004, ApJ, 616, 71

Swinbank A. M., Smail I., Chapman S. C., Blain A. W., Ivison R. J., Keel W. C., 2004, ApJ, 617, 64

Swinbank A. M. et al., 2005, MNRAS, 359, 401

Tacconi L. J., Genzel R., Tecza M., Gallimore J. F., Downes D., Scoville N. Z., 1999, ApJ, 524, 732

Tacconi L. J. et al., 2006, ApJ, 640, 228

Tecza M. et al., 2004, ApJ, 605, L109

Veilleux S., Osterbrock D. E., 1987, ApJS, 63, 295

Webb T. M. et al., 2003a, ApJ, 587, 41

Webb T. M. A., Lilly S. J., Clements D. L., Eales S., Yun M., Brodwin M., Dunne L., Gear W. K., 2003b, ApJ, 597, 680

This paper has been typeset from a T$_{\rm E}$X/L$^{\rm A}$T$_{\rm E}$X file prepared by the author.